Biomaterials Science

ROYAL SOCIETY OF CHEMISTRY

PAPER

View Article Online
View Journal | View Issue

Cite this: *Biomater. Sci.*, 2021, **9**, 7575

Magnetic and radio-labeled bio-hybrid scaffolds to promote and track *in vivo* the progress of bone regeneration†

Elisabetta Campodoni, *[a] Marisela Velez,*[b] Eirini Fragogeorgi,[c,d] Irene Morales,[e,f] Patricia de la Presa,[e,f] Dimitri Stanicki,[g] Samuele M. Dozio,[a,h] Stavros Xanthopoulos,[c] Penelope Bouziotis,[c] Eleftheria Dermisiadou,[d] Maritina Rouchota,[d] George Loudos,[c,d] Pilar Marín,[e,f] Sophie Laurent,[g,i] Sébastien Boutry,[g,i] Silvia Panseri,[a] Monica Montesi,[a] Anna Tampieri[a] and Monica Sandri*[a]

This work describes the preparation, characterization and functionalization with magnetic nanoparticles of a bone tissue-mimetic scaffold composed of collagen and hydroxyapatite obtained through a biomineralization process. Bone remodeling takes place over several weeks and the possibility to follow it *in vivo* in a quick and reliable way is still an outstanding issue. Therefore, this work aims to produce an implantable material that can be followed *in vivo* during bone regeneration by using the existing non-invasive imaging techniques (MRI). To this aim, suitably designed biocompatible SPIONs were linked to the hybrid scaffold using two different strategies, one involving naked SPIONs (nMNPs) and the other using coated and activated SPIONs (MNPs) exposing carboxylic acid functions allowing a covalent attachment between MNPs and collagen molecules. Physico-chemical characterization was carried out to investigate the morphology, crystallinity and stability of the functionalized materials followed by MRI analyses and evaluation of a radiotracer uptake ([^{99m}Tc]Tc-MDP). Cell proliferation assays *in vitro* were carried out to check the cytotoxicity and demonstrated no side effects due to the SPIONs. The achieved results demonstrated that the naked and coated SPIONs are more homogeneously distributed in the scaffold when incorporated during the synthesis process. This work demonstrated a suitable approach to develop a biomaterial for bone regeneration that allows the monitoring of the healing progress even for long-term follow-up studies.

Received 1st June 2021,
Accepted 30th September 2021

DOI: 10.1039/d1bm00858g

rsc.li/biomaterials-science

1. Introduction

Bone is a connective tissue responsible for supporting and protecting organs and facilitating mobility. There are many situations in a lifespan that can induce bone defects: trauma, tumors, infections, natural aging, bone fractures, obesity and lack of physical activity.[1] Fortunately, unlike other tissues, bone can regenerate and repair itself without scars when the damage is limited in size. However, if the defect caused by a severe pathological condition is too extended, bone healing and repair can fail.[2] Alternatives, in such cases, can be several forms of bone grafts, defined as implantable materials that promote bone healing alone or in combination with other materials, such as *ad-hoc* designed three-dimensional (3D) porous structures that mimic and share the essential properties of natural bone. These substitute materials should be thoroughly characterized in terms of porosity, compression resistance, biodegradation, biocompatibility and interaction

[a]*Institute of Science and Technology for Ceramics-National Research Council (CNR), Faenza, Italy. E-mail: elisabetta.campodoni@istec.cnr.it*
[b]*Instituto de Catálisis y Petroleoquímica (CSIC), Madrid, Spain. E-mail: marisela.velez@icp.csic.es*
[c]*National Center for Scientific Research (NCSR) "Demokritos", Institute of Nuclear & Radiological Sciences & Technology, Energy &Safety, Ag. Paraskevi-Athens, Greece*
[d]*BIOEMTECH, Lefkippos Attica Technology Park, NCSR "Demokritos", Ag. Paraskevi-Athens, Greece*
[e]*Instituto de Magnetismo Aplicado (UCM-ADIF-CSIC), A6 22, Las Rozas, 28260, Spain*
[f]*Dpto Física de Materiales, UCM, Ciudad Universitaria, Madrid, 28040, Spain*
[g]*University of Mons, General, Organic and Biomedical Chemistry, NMR and Molecular Imaging Lab, 7000 Mons, Belgium*
[h]*Institute of Solid-State Electronics, Vienna University of Technology, Vienna, Austria*
[i]*Center for Microscopy and Molecular Imaging, 6041 Charleroi, Belgium*
†Electronic supplementary information (ESI) available. See DOI: 10.1039/d1bm00858g

with cells *in vitro* before moving to pre-clinical *in vivo* studies and clinical trials. Moreover, as bone is a dynamic tissue that constantly remodels, specific investigations are needed to assess bone self-healing and correct graft placement during implantation *in vivo*. This progress can be made using histological techniques, but they are time-consuming, labor-intensive, invasive and destructive analyses and require the use of a large number of animals. Non-invasive imaging techniques are essential to perform this evaluation and several options are available to monitor the repair and fate of host–material interactions and to follow the evolution of the implanted materials over time *in vivo.*[3] X-ray computed tomography (CT), nuclear imaging (single photon emission computed tomography SPECT and positron emission tomography PET) and magnetic resonance imaging (MRI) of bone are some of the most frequently used techniques. SPECT and PET imaging rely on the detection of photons emitted from radioisotopes alone or combined with chemical and biologically active substances (radiotracers) that must previously be incorporated into the scaffold.[4] Since the sensitivity of the techniques is very high, the small amounts of radiotracers, at the nano- or pico-molar level (10^{-9}, 10^{-10}, 10^{-12} M), needed for the detection, are not toxic to the organism. However, the *in vivo* life-time of radiotracers is rather short and therefore they require repeated administrations over time, usually once per week.

MRI of bone also requires incorporation of contrast agents into the scaffold. This imaging technique is based on the presence of a non-ionizing proton (^{1}H) and provides high resolution imaging of unlimited depth in soft tissues rich in water. Structures lacking a high water percentage (such as hard bone or air) appear light and lack a good MRI signal that can be improved by the addition of exogenous contrast agents into the scaffold. The use of both SPECT and MR imaging techniques would allow tracking bone regeneration at different time scales: short term with nuclear imaging (SPECT), and longer time scales with magnetic imaging (MRI).

Based on the scenario described above, this work deals with the preparation of a biomimetic hybrid scaffold for bone regeneration and its functionalization with magnetic nanoparticles and a radioactive label to allow the use of nuclear and magnetic resonance imaging (MRI, SPECT, PET) for its visualization when implanted *in vivo.* This will therefore allow following the progress of bone tissue regeneration without the use of invasive methodologies also for long-term follow-up.

The hybrid scaffolds (HyS) involved in this study are obtained through biomineralization, the process which occurs in nature to form minerals in hybrid materials such as bone, and closely mimic the native tissue chemical composition and their 3D porous morphology, required to host cells, to reconstruct new healthy tissue and allow the subsequent and progressive resorption of the implanted scaffold.[3,5] In particular, as they contain organic biopolymers and minerals, they have unique properties that give rise to complex architectures and functions.[6,7] In detail, bone-like hydroxyapatite nanocrystals are nucleated on self-assembling collagen fibers, the protein present in bone tissue and tendon, and serve as a template guiding the biomineralization process. The extent and morphology of the pores in the formed hybrid composite, usually ranging between 80 and 85%, can be customized by the final freeze-drying step.[1,6–10] This synthetic process allows also the inclusion of foreign and mimetic ions in the hydroxyapatite crystals formed on collagen molecules. This appropriate morphology, composition and orientation of the apatite favor cell recognition, adhesion and proliferation on the scaffolds preventing undesired inflammatory reactions, as largely demonstrated by previous studies.[10] In this work the regenerative performances of the developed hybrid materials (HyS) were previously evaluated *in vivo* by using a commercial radiolabel ([^{99m}Tc]Tc-MDP) and SPECT/CT techniques that showed their efficiency in terms of signal intensity. These studies confirmed their previously well-established biocompatibility and, at the same time, their suitability for allowing the visualization of the regeneration progress, providing an accurate tool for monitoring the bone healing process.

Then, superparamagnetic iron oxide nanoparticles (SPIONs) are obtained by the polyol method, which consisted of the co-precipitation of metal oxide in high boiling alcohol.[11] They are chosen for their wide use in the past decades in medical and clinical fields for imaging and therapeutics, and here were used to label the hybrid bone scaffolds. In this work two different SPIONs were involved: naked SPIONs (nMNPs) physically entrapped in the hybrid composite during the synthesis, and coated and activated newly patented SPIONs (MNPs), modified with activated carboxylic groups on the surface to promote covalent attachment with a hybrid composite.[12,13]

This research study focused on the preparation and characterization of bone-like hybrid scaffolds and on the optimization of the protocol for their labeling with SPIONs. Different approaches were investigated to achieve homogeneous and effective functionalization with nMNPs and MNPs without losing the excellent properties and the biocompatibility of the hybrid composite. To this aim, physico-chemical characterization was carried out to investigate the features of functionalized materials in terms of composition, crystallinity and morphology, followed by cytotoxicity tests *in vitro* and preliminary functionality tests *in vivo* with SPECT and CT techniques. Finally, MRI *in vitro* studies allowed the visualization of the functionalized-HySs demonstrating the effectiveness of the labelling protocols.

2. Materials and methods

Equine tendon derived type I collagen gel (Coll), 1 wt% in aqueous acetic buffered solution (pH 3.5), was purchased from Opocrin SpA (Italy). Phosphoric acid (H_3PO_4, 85 wt%), calcium hydroxide ($Ca(OH)_2$, 95 wt%), magnesium chloride hexahydrate ($MgCl_2{\cdot}6H_2O$, 99 wt%), *N*-(3-dimethylaminopropyl)-*N*′-ethylcarbodiimide hydrochloride (EDC) and *N*-hydroxysulfosuccinimide sodium salt (sulfo-NHS, >98%)

were purchased from Sigma Aldrich (USA). Phosphate buffer saline (PBS, pH 7.4) was supplied by EuroClone (Italy). [^{99m}Tc], obtained in physiological saline as [^{99m}Tc]$NaTcO_4$, was eluted from a commercial [^{99}Mo]/[^{99m}Tc] generator (6GBq, Tekcis, CuriumTM (FR)). Methylene-diphosphonate (PolTechMDP kit, 5 mg) reconstituted with 3 mL of freshly eluted [^{99m}Tc]$NaTcO_4$ solution (90 mCi or 3330 MBq) from the generator, in the form of [^{99m}Tc]Tc-MDP for testing binding affinity towards scaffolds was purchased from Polatom (PL). ITLC analysis of [^{99m}Tc]Tc-MDP was performed on a radio TLC detector (miniGITA TLC scanner, Elysia-Raytest (BE)). A radioisotope dose calibrator (Capintec, Inc. (US)) was used for measuring radioactivity. Radiochemical quality control was performed with glass microfiber chromatography paper impregnated with a silica gel (ITLC-SG) (Agilent Technologies (US). Ferric chloride solution ($FeCl_3$, 45%), ferrous chloride tetrahydrate ($FeCl_2{\cdot}4H_2O$, >99%) and sodium hydroxide were purchased from Fluka (Belgium). Diethyleneglycol (DEG), dimethylformamide (DMF), acetone and diethylether were purchased from Sigma-Aldrich (Belgium) while 3-(triethoxysilyl)propyl succinic anhydride (TEPSA) was purchased from ABCR (Germany). All the materials mentioned above were used without further purification. Membranes (MWCO = 30 kDa) for ultrafiltration were purchased from Millipore (USA).

2.1. Synthesis of superparamagnetic iron oxide nanoparticles

2.1.1 Synthesis of naked SPIONs (nMNPs). Superparamagnetic iron oxide nanoparticles (SPIONs) were prepared by co-precipitation of iron salts in DEG according to a protocol previously described.[11] Briefly, a mixture of ferrous chloride tetrahydrate salt (45 mmol; 8.9 g) and ferric chloride (45%; 37 mmol; 9.1 ml) in DEG (250 ml) was heated at 170 °C under stirring. Sodium hydroxide (15 g) was then added and the solution was kept at 170 °C for 1 hour. The mixture was then cooled, and the magnetic particles were isolated from the solution by magnetic decantation, after which the black precipitate was washed several times with nitric acid (1 M). The particles were finally dispersed in deionized water, sonicated (45 minutes), and centrifuged (16 500*g*; 45 min).

2.1.2 Synthesis of activated SPIONs (MNPs). Superparamagnetic iron oxide nanoparticles (SPIONs) were prepared by co-precipitation of iron salts in DEG according to a protocol previously described.[11] Briefly, a mixture of ferrous chloride tetrahydrate salt (45 mmol; 8.9 g) and ferric chloride (45%; 37 mmol; 9.1 ml) in DEG (250 ml) was heated at 170 °C under stirring. Sodium hydroxide (15 g) was then added and the solution was kept at 170 °C for 1 hour. The mixture was then cooled, and the magnetic particles were isolated from the solution by magnetic decantation, after which the black precipitate was washed several times with nitric acid (1 M). The particles were finally dispersed in deionized water, sonicated (45 minutes), and centrifuged (16 500*g*; 45 min). The resulting suspension (20 ml; [Fe] = 250 mM) was diluted in DMF (50 ml) and water was removed under reduced pressure. TEPSA (25 mmol; 7.1 ml) was then added to the nanoparticle dispersion in DMF, followed by water (4.3 ml), and TMAOH (1 M; 2.5 mmol; 2.5 ml). The suspension was heated at 100 °C for 24 h under continuous stirring. The as-modified particles were collected after pouring the suspension in an acetone–diethylether mixture and then were purified by means of membrane filtration (membrane cut-off: 30 kDa). The content of carboxylic moieties was estimated by conductimetric titration, yielding a molar ratio of 2.4 mol% acidic functions compared to the total iron content.

The total iron concentration was determined by measuring the longitudinal relaxation rate $R1$ according to the method previously described.[14] Briefly, the samples were mineralized by microwave assisted digestion (MLS-1200 Mega, Milestone, Analis, Belgium) and the $R1$ value of the resulting solutions was recorded at 0.47 T and 37 °C, which allowed the determination of iron concentration using the equation:

$$[\mathrm{Fe}] = (R1_{\mathrm{sample}} - R1_{\mathrm{dia}}) \times 0.0915$$

where $R1_{\mathrm{dia}}$ (s^{-1}) is the diamagnetic relaxation rate of acidified water (0.36 s^{-1}) and 0.0915 (s mM) is the slope of the calibration curve.

Measurements of the size distribution and zeta potential of nanoparticles suspended in aqueous medium were performed on a Zetasizer Nano ZS (Malvern Instruments, United Kingdom) using a laser He–Ne (633 nm). The zeta potential was determined directly in a solution containing NaCl (0.01 mM). The pH of the aqueous suspension was adjusted by adding 0.1–0.001 mM HNO_3 or TMAOH solution.

MNPs have been obtained through the activation of external functional groups of the TEPSA shell by EDC/sulfo-NHS coupling following a published procedure.[13,15] Briefly, 72.27 mg of EDC and 50.54 mg of sulfo-NHS were simultaneously added to 4.84 mL of TEPSA-SPIONs (370 mM) at room temperature and the suspension was shaken for 1 hour in order to obtain MNPs.

2.2. Development of magnetically functionalized hybrid scaffolds

Hybrid scaffolds (HyS), composed of collagen (Coll) and magnesium-doped hydroxyapatite (HA) obtained through a biomineralization process,[16] have been synthesized with a HA/Coll weight ratio of 70/30 and selected because they are similar to the composition of natural bone tissue.

Two types of magnetic nanoparticles were used to functionalize HyS: naked SPIONs (nMNPs) that were expected to get mechanically trapped in the scaffold, and modified SPIONs (MNPs), designed to covalently attach to the collagen fibers.

Three different strategies for including both magnetic nanoparticles into the scaffold were explored: (1) linking nanoparticles with collagen gel before synthesizing the HyS through the biomineralization process ((MNPs)HyS and (nMNPs)HyS); (2) adding nanoparticles during the biomineralization process in order to simultaneously promote the synthesis of the HyS and the functionalization with magnetic nanoparticles (Hy(MNPs)S and Hy(nMNPs)S); (3) soaking in

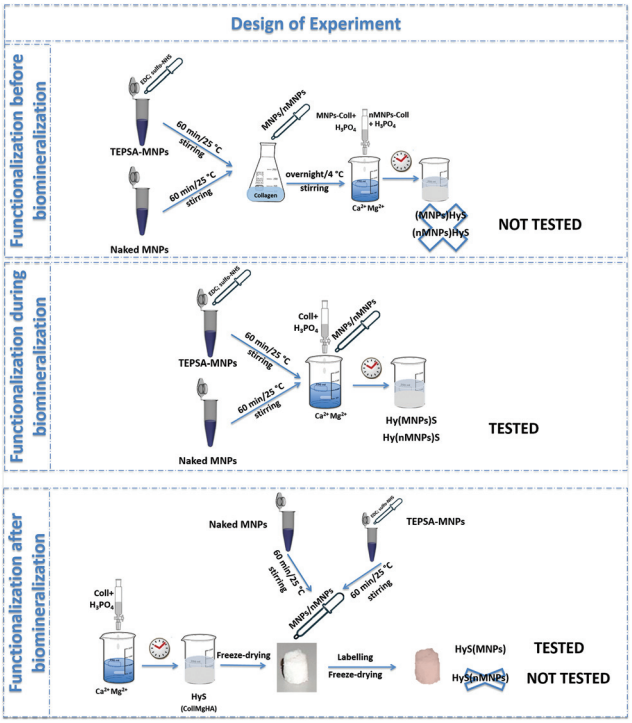

Scheme 1 Representation of the different approaches used to magnetically functionalize hybrid scaffolds (HyS). All materials represented here are obtained by three different functionalization approaches: before, during and after biomineralization synthesis process. Samples signed with a cross (X) have been discarded during preliminary screening stages.

the suspension of nanoparticles after synthesizing the HyS through the biomineralization process (HyS(MNPs) and HyS (nMNPs)) (Scheme 1)‡.

2.2.1. Synthesis of hybrid scaffolds as control samples (HyS). Briefly, 100 g of collagen gel were diluted with 350 mL of phosphoric acid solution (0.04 M), while 0.235 g of $MgCl_2 \cdot 6H_2O$ were added to 330 mL of basic calcium suspension (0.07 M).[16] The acid collagen slurry was added dropwise into the basic calcium and magnesium suspension, leading to the formation of Mg-doped apatite nanocrystals uniformly distributed in the collagen matrix. After 2 h at room temperature, the hybrid slurry was washed three times in distilled water and filtered to remove free ions before pouring it into a polystyrene 96-well plate. Porous 3D hybrid scaffolds were obtained by freezing the slurry at −40 °C with a controlled freezing ramp of 50 °C h^{-1} and drying it with two heating ramps, 5 °C h^{-1} up to −5 °C and 2 °C h^{-1} up to 20 °C (5 Pascal, LIO 3000 PLT, Italy) for 48 h under a constant vacuum of 0.086 mbar. Finally, the scaffolds were sterilized by gamma-irradiation.

2.2.2. Synthesis of hybrid scaffolds functionalized with magnetic nanoparticles before biomineralization: (MNPs)HyS and (nMNPs)HyS. Briefly, 100 g of collagen gel were diluted with 500 mL of milliQ water. The magnetic solution was prepared diluting 4.84 mL of MNPs (previously activated as reported in paragraph 2.1) in 100 mL of HEPES (0.16 M) or diluting 4.71 mL of nMNPs in 100 mL of HEPES (0.16 M). MNPs/nMNP solutions were added into the collagen slurry under magnetic stirring at 4 °C and remained under these conditions for two hours.

After that, magnetically functionalized collagen was washed and filtered twice in distilled water before being diluted in 350 mL of phosphoric acid solution (0.04 M). At the same time, 0.235 g of $MgCl_2 \cdot 6H_2O$ were added to 330 mL of basic calcium suspension (0.07 M).[16] Finally, acid and magnetically functionalized collagen was added dropwise into the basic calcium and magnesium suspension, leading, theoretically, to the formation of Mg-doped apatite nanocrystals uniformly distributed in the collagen matrix and functionalized with MNPs or nMNPs. After 2 h at room temperature, the hybrid and magnetic slurry was gently shaken for two hours, washed three times in distilled water and filtered to remove free ions before pouring it into a polystyrene 96-well plate. Porous 3D hybrid and magnetic scaffolds were obtained by freezing the slurry at −40 °C with a controlled freezing ramp of 50 °C h^{-1} and drying it with two heating ramps, 5 °C h^{-1} up to −5 °C and 2 °C h^{-1} up to 20 °C (5 Pascal, LIO 3000 PLT, Italy) for 48 h under a constant vacuum of 0.086 mbar. Finally, the scaffolds were sterilized by gamma-irradiation.

2.2.3. Synthesis of hybrid scaffolds functionalized with magnetic nanoparticles during biomineralization: Hy(MNPs)S and Hy(nMNPs)S. Briefly, 100 g of collagen gel were diluted with 350 mL of phosphoric acid solution (0.04 M), while 0.235 g of $MgCl_2 \cdot 6H_2O$ were added to 330 mL of basic calcium suspension (0.07 M).[16] The magnetic solution was prepared diluting 4.84 mL of MNPs (previously activated as reported in paragraph 2.1) in 100 mL of HEPES (0.16 M) or diluting 4.71 mL of nMNPs in 100 mL of HEPES (0.16 M). The acid collagen slurry and MNPs/nMNP solution were simultaneously added dropwise into the basic calcium and magnesium suspension, leading to the formation of Mg-doped apatite nanocrystals uniformly distributed in the collagen matrix and functionalized with MNPs or nMNPs. After 2 h at room temperature, the hybrid and magnetic slurry was gently shaken for two hours, washed three times in distilled water and filtered to remove free ions before pouring it into a polystyrene 96-well plate. Porous 3D hybrid and magnetic scaffolds were obtained by freezing the slurry at −40 °C with a controlled freezing ramp of 50 °C h^{-1} and drying it with two heating ramps, 5 °C h^{-1} up to −5 °C and 2 °C h^{-1} up to 20 °C (5 Pascal, LIO 3000 PLT, Italy) for 48 h under a constant vacuum of 0.086 mbar. Finally, the scaffolds were sterilized by gamma-irradiation.

2.2.4. Synthesis of hybrid scaffolds functionalized with magnetic nanoparticles after biomineralization: HyS(MNPs) and HyS(nMNPs). Briefly, 100 g of collagen gel were diluted with 350 mL of phosphoric acid solution (0.04 M), while 0.235 g of $MgCl_2 \cdot 6H_2O$ were added to 330 mL of basic calcium suspension (0.07 M).[16] The acid collagen slurry was added dropwise into the basic calcium and magnesium suspension,

‡The order in which MNP and HyS appears in the name refers to whether the particles were added before, during or after fabricating the scaffold.

leading to the formation of Mg-doped apatite nanocrystals uniformly distributed in the collagen matrix. After 2 h at room temperature, the hybrid slurry was washed three times in distilled water and filtered to remove free ions before pouring it into a polystyrene 96-well plate. Porous 3D hybrid scaffolds were obtained by freezing the slurry at −40 °C with a controlled freezing ramp of 50 °C h^{-1} and drying it with two heating ramps, 5 °C h^{-1} up to −5 °C and 2 °C h^{-1} up to 20 °C (5 Pascal, LIO 3000 PLT, Italy) for 48 h under a constant vacuum of 0.086 mbar. Afterwards, each scaffold was soaked in a specific amount of MNPs or nMNPs (previously activated as reported in paragraph 2.1) depending on the scaffold weight in order to obtain a functionalization of 3 wt% (g Fe per g scaffold). Finally, the scaffolds were freeze-dried following the previous cycle and sterilized by gamma-irradiation.

2.3. Characterization of hybrid and magnetic scaffolds

Complete characterization was performed to analyze and quantify the mineral phases in the scaffolds and evaluate their structure, porosity and magnetic properties while their signals at MRI were also investigated. Furthermore, a preliminary *in vivo* study was performed to evaluate the effective regenerative potential of the hybrid scaffold (HyS) by radiolabeling with ([^{99m}Tc]Tc-MDP and following the *in vivo* life cycle using SPECT and CT techniques. Then, an *in vitro* investigation was carried out to evaluate if the addition of MNPs or nMNPs affected the cytotoxicity of the hybrid scaffolds (HyS). Once the most appropriate scaffolds were selected on the basis of this characterization, we proceeded to radiolabel them, in order to evaluate the use of SPECT imaging for tracking the *in vivo* life cycle.

2.3.1. *In vivo* evaluations: SPECT and CT imaging. Animals used for the imaging studies were obtained from the breeding facilities of the Institute of Biosciences and Applications, National Center for Scientific Research "Demokritos". The experimental facility of the Radiochemistry Studies Laboratory is registered according to the Greek Presidential Decree 56/2013 (Reg. Number: EL 25 BIO 022), in accordance with National Legislation, which is harmonized with the European Directive 2010/63, on the protection of animals used for scientific purposes. All applicable national guidelines for the care and use of animals were followed. The study protocol was approved by the Department of Agriculture and Veterinary Service of the Prefecture of Athens (Protocol Number: 6333/21-11-2018). Mice were kept under controlled conditions in a ventilated IVC cage system at constant temperature (22 ± 2 °C) and humidity (45–50%) and were housed under a 12 h light/dark cycle, with free access to commercial pellet food and tap water. Imaging studies were performed on a mouse defect calvarial model that was created for this purpose. Two symmetrical calvarial bone defects, 1.5 mm in diameter each, were created in female Swiss mice. Gaps were monitored weekly through SPECT/CT imaging, using [^{99m}Tc]Tc-MDP for 5 weeks. Defects created on the left part of the mouse skull were left unfilled (control group), whereas those on the right part were filled with mineralized horse collagen scaffold materials (HyS). Tomographic SPECT/CT imaging was performed with y-CUBETM and x-CUBETM (Molecubes, Belgium), respectively, after three hours p.i. of 2 mCi of [^{99m}Tc]Tc-MDP. The SPECT system provides a spatial resolution of 0.6 mm for mouse imaging and of 1.5 mm for rat imaging. The CT system performs a spiral scan and can provide images with 50 μm resolution and it operates between 35 and 80 kVp, with a 10–500 μA tube current. Mouse imaging was performed by keeping the mice anesthetized under isoflurane and at a constant temperature of 37 °C. SPECT scans were acquired with a 30–40 min duration, and each SPECT scan was followed by a High-Resolution CT scan for co-registration purposes. The SPECT data were reconstructed through an MLEM algorithm, with 250 μm voxel size and 500 μm iterations. Images were decay corrected and normalized between different scans. CT data were reconstructed through an ISRA algorithm, with 100 μm voxel size. CT imaging showed the actual bone filling process and the formation of new bone tissue, whereas SPECT imaging provided information on increased metabolic activity.

2.3.2. Chemical–physical characterization. The quantitative determination of Mg^{2+}, Ca^{2+}, $Fe^{2+/3+}$ and PO_4^{3-} ions present in the scaffolds and constituting the mineral component was measured by inductively coupled plasma-optical emission spectrometry (ICP-OES, Agilent Technologies 5100 ICP-OES, Santa Clara, USA). Briefly, 30 mg of the hybrid composite was subjected to 2 ml nitric acid (65 wt%) digestion followed by subsequent sonication and dilution with 100 ml of Milli-Q water (n = 3). The following analytical emission wavelengths were used for ion quantification: Ca (422 nm); Mg (279 nm); Fe (259 nm); and P (214 nm).

FTIR spectra in the attenuated total reflection mode (FTIR-ATR) were collected on a Nicolet iS5 spectrometer (Thermo Fisher Scientific Inc, Waltham, MA, USA) with a resolution of 4 cm^{-1} by accumulation of 64 scan covering the 4000 to 400 cm^{-1} range using a diamond ATR accessory model iD7 (n = 3).

The X-ray diffraction (XRD) patterns of the samples were recorded by using a D8 Advance diffractometer (Bruker, Karlsruhe, Germany) equipped with a Lynx-eye position-sensitive detector (Cu Kα radiation, λ = 1.54178 Å) generated at 40 kV and 40 mA. XRD spectra were recorded in the 2θ range from 20° to 60° with a step size (2θ) of 0.02° and a counting time of 0.5 s (n = 3).

Thermal properties and the ratio between organic and inorganic phases were measured using a simultaneous thermal analyzer STA 449/C Jupiter (Netzsch, Germany). Briefly, 20 mg of the hybrid composite were placed in an alumina crucible and then brought from room temperature to 1100 °C at a heating rate of 10° C min^{-1} in airflow of 30 mL min^{-1} (n = 3).

2.3.3. Morphological and dimensional properties. The topographical micro-architecture of the composites was examined by environmental scanning electron microscopy (ESEM, Quanta 200 FEG, FEI Company, Hillsboro, OR, USA) performed on sample specimens mounted onto aluminum stubs using black carbon tapes and sputter coated with gold (Polaron Sputter Coater E5100, Watford, Hertfordshire, UK).

The total porosity of the scaffolds was calculated by the density method[17] according to the formula:

$$\text{total porosity}\,(\%) = 100 - \left(\frac{\rho}{\rho_{\text{theoretical}}} \times 100\right)$$

where ρ is the scaffold density determined with the following equation:

$$\rho = \frac{W}{\pi \times \left(\frac{D}{2}\right)^2 \times H}$$

in which W is the weight, D is the diameter and H is the height of the scaffold.

The theoretical density of the material is calculated from the theoretical density and weight fraction (X_A, X_B *etc.*) of each reagent in the following way:

$$\rho_{\text{theoretical}} = (\rho_{\text{theoretical(A)}} \times X_A) + (\rho_{\text{theoretical(B)}} \times X_B)$$

all values were expressed as the mean ± SEM (n = 3).

The macropore volume percentage was calculated by the water squeezing method.[18] Briefly, the scaffold was equilibrated in deionized water for one hour and weighed (M_{swollen}), then squeezed to remove the water filling pores and weighed again (M_{squeezed}).

The macropore volume was calculated using the following equation:

$$\text{macroporosity}\,(\%) = \frac{M_{\text{swollen}} - M_{\text{squeezed}}}{M_{\text{swollen}}} \times 100$$

All values were expressed as the mean ± SEM (n = 3).

The fluid uptake ability of scaffolds was evaluated through the swelling test under physiological conditions (in PBS solution at 37 °C). In brief, dried scaffolds were immersed in PBS solution at 37 °C. At specific time points scaffolds were withdrawn carefully, the excess of moisture was removed and the weight was measured. The swelling ratio was calculated as follows:

$$Q_s = \frac{W_s - W_d}{W_d}$$

where W_s is the weight of the swollen sample at a specific time point and W_d is the initial weight of the dried sample. All values were expressed as the mean ± SEM (n = 3).

The stability of scaffolds under physiological conditions (PBS solution at 37 °C) was evaluated through the degradation test in which previously weighed scaffolds were soaked in PBS at 37 °C. At specific time points, scaffolds were washed twice with deionized water, freeze-dried and subsequently weighed. The degradation percentage (D) was evaluated using the following equation:

$$D(\%) = \frac{W_i - W_f}{W_i} \times 100$$

where W_i is the initial weight of the dried scaffold and W_f is the weight of the freeze-dried scaffold at a specific time point. All values were expressed as the mean ± SEM (n = 3).

2.3.4. Magnetic characterization. Magnetic characterization has been performed in a Quantum Design MPMS-5S SQUID magnetometer. Zero field cooled (ZFC) and field cooled (FC) curves have been recorded from 5 to 300 K at 100 Oe applied field. Hysteresis loops of powder samples have been measured at 5 and 300 K and at 50 kOe maximum applied field.

MRI was performed with a Bruker Biospec 9.4 T scanner (Karlsruhe, Germany), using a 40 mm volume coil. Scaffolds were water-immersed in 0.5 ml tubes which were also placed in a water-filled 50 ml tube. Signal darkening induced by MNPs within the scaffolds was visualized with a 3D-ultrashort echo time (UTE) sequence (TR = 5 ms, TE = 35 μs, NEX = 5, resolution = 208 × 208 micrometers, slice thickness = 1 mm).

2.4. *In vitro* evaluations

2.4.1. *In vitro* cell growth. The human osteoblast cell line (hFOB 1.19 ATCC® CRL-11372™) was cultured in Dulbecco's Modified Eagle's Medium with no phenol red (DMEM/F12, Gibco), supplemented with gentamicin (G418 0.3 mg ml^{-1}) and 10% fetal bovine serum (FBS). Cultured cells were kept at 37 °C under an atmosphere of 5% CO_2. Cells were detached by trypsinization and centrifuged. After the detachment from culture flasks, the cell number and viability were assessed with the trypan blue dye exclusion test. The scaffolds were sterilized by 25 kGy γ-ray irradiation and placed in a 24-well plate for pre-soaking in culture medium for 24 hours. The seeding process of the cells was performed by carefully dropping a 30 μL cell suspension (5.0×10^4 cells) onto the scaffolds. The seeded cells were incubated for 30 min to allow cell adhesion before adding 1.5 mL of cell culture medium into each well. The medium was changed every 3 days. All cell handling procedures were performed in a sterile laminar flow hood. All incubation steps were performed at 37 °C with 5% CO_2.

2.4.2. Cell viability assay. Cell viability was quantified using the XTT assay (sodium 3′-[1-(phenylaminocarbonyl)-3,4-tetrazolium]-bis (4-methoxy-6-nitro) benzene sulfonic acid hydrate, 5 mg mL^{-1}). Following the manufacturer's instructions, XTT was added directly into the wells containing the seeded scaffolds in a 1 : 10 proportion to the present cell culture medium. This procedure was performed at each time point (1, 3 and 7 days). After 2 h of incubation at 37 °C and 5% CO_2, the medium containing the dissolved formazan salts is transferred into a 96-well plate and the absorbance is read at 450 nm using a Multiskan FC Microplate Photometer (Thermo Scientific). The registered absorbance was directly proportional to the number of metabolically active cells. For each time point, three samples were used and analyzed in technical triplicate.

Qualitative cell viability was assessed using the Live/Dead assay kit (Invitrogen), used according to the manufacturer's instructions. At each time point (1, 3 and 7 days), a sample for each scaffold composition was washed with PBS 1× for 5 min and incubated with 2 μM calcein acetoxymethyl (calcein AM) plus 4 μM ethidium homodimer-1 (EthD-1) for 15 min at 37 °C in the dark. Samples were rinsed in PBS 1× and images were

acquired using an inverted Ti–E fluorescence microscope (Nikon).

2.4.3. Cell morphology analysis. Cell morphology of hFOB seeded on to the scaffolds was evaluated at day 7 by actin/nuclei fluorescent staining and detection *via* a fluorescence microscope. Briefly, the samples were washed in PBS 1× for 5 min and fixed in 4% (w/v) paraformaldehyde for 15 min. Permeabilization was performed with PBS 1× with 0.1% (v/v) Triton X-100 for 5 min, and actin filaments were highlighted with FITC-conjugated phalloidin (Invitrogen, 38 nM) staining followed by DAPI nuclear staining (Invitrogen, 300 nM) and visualized with an inverted Ti–E fluorescence microscope (Nikon).

2.5. Radiolabeling analysis

The rate of binding affinity of the SPECT bone imaging tracer, [^{99m}Tc]-MDP, towards the magnetic hybrid scaffolds, Hy(MNPs)S, was investigated at two different concentrations of MNPs, 1.5 wt% (MNPs_1.5%) and 0.75 wt% (MNPs_0.75%). Therefore, the magnetic hybrid 3D scaffold was first weighed (~15 mg), then immersed in an aqueous medium of a final volume of 1 ml containing 50 μl [^{99m}Tc]-MDP (1500 μCi or 55.5 MBq which corresponds to ~100 μg of "cold" MDP) and incubated at 37 °C for 15 min, 3 h and 5 h. For each of the time points tested, the scaffold was extracted from the media and the radioactivity of both the media and scaffold was measured in a dose calibrator, and then the scaffold was re-immersed in the media. The not magnetized scaffold (HyS) was used as a control sample. To check if the SPECT tracer remains intact under the above-mentioned conditions, its stability was evaluated at 15 min, 3 h and 5 h *via* instant thin layer chromatography using ITLC-SG as the stationary phase and methyl-ethyl ketone (MEK) as the mobile phase. Finally, paper strips were dried at room temperature and were read for 2 min on a Radio-TLC scanner.

3. Results and discussion

3.1. Different approaches to functionalize hybrid scaffolds

In this work we have prepared biomimetic hybrid scaffolds (magnesium-doped hydroxyapatite mineralized on collagen fibers) functionalized with magnetic nanoparticles (SPIONs).[1,9] Several research studies have previously demonstrated the ability of this hybrid material to recreate *in vivo* a perfect microenvironment suitable and effective for bone regeneration.[19,20] Nevertheless, before proceeding to its magnetic functionalization, we first confirmed that this hybrid scaffold can promote bone regeneration and that we could follow it *in vivo* using SPECT and CT imaging. Fig. 1 shows SPECT and CT data acquired up to 5 weeks after calvarial bone defect surgery, demonstrating that HyS effectively induced bone regeneration at this specific implantation site. SPECT imaging revealed the increased metabolic activity by using the radioactive tracer [^{99m}Tc]Tc-MDP, which has high affinity for the inorganic component of bones, whereas CT imaging

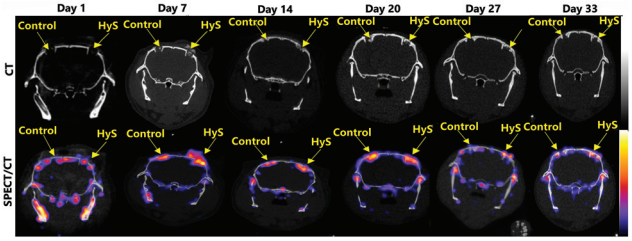

Fig. 1 Imaging results on day 1, 7, 14, 20, 27 and 33 post-surgery. Coronal views of the control defect (left) and of HyS filled defect (right). 1st row: CT images on the skull of a Swiss Albino mouse model; 2nd row: fused SPECT/CT images at 3 h post-injection with the bone imaging tracer [^{99m}Tc]Tc-MDP (~2 mCi).

showed the actual bone filling process and the formation of new bone tissue over time. More specifically, for the HyS treated defect, a peak in metabolic activity was noted on day-7 post-surgery without a significant change up to day 20 with [^{99m}Tc]Tc-MDP uptake starting to decrease on days 27 and 33. In contrast, the metabolic activity of the control animal, where no scaffold was introduced in the defect area, was stable but significantly lower and complete healing was not observed up to day 33 post-surgery. Clear visualization was achieved on both defects *via* CT imaging during the first week post-surgery and signs of new bone formation were clearly observed on day 20. Thus, CT is shown to be a high-resolution tool for controlling new bone formation and SPECT is a high sensitivity tool for early confirmation of metabolic activity, also having a high prognostic value for bone healing. In order to allow for a long term follow up of the regenerative process[4,21] the hybrid scaffold has been labelled with MNPs to detect it by MRI. Another purpose of MNP labelling is to enhance the ability to induce cell proliferation and osteogenic differentiation both *in vitro* and *in vivo*. Bone fracture healing and bone ingrowth are boosted by weak magnetic or pulsed electromagnetic fields,[22] but even in the absence of a magnetic field, magnetic scaffolds have been shown to have a positive effect on regeneration.[23]

Because of their remarkable bio- and physico-chemical properties (*i.e.* poor toxicity, biocompatibility, strong magnetic moment) magnetic iron oxide nanoparticles (SPIONs) were chosen to label the as-proposed scaffold.[24] Specifically, two different nanoparticles were selected: (i) naked SPIONs (nMNPs) and (ii) modified/activated SPIONs (MNPs). MNPs were obtained by means of a two-step procedure which implied first the preparation of the magnetic cores by co-precipitation in organic media (*i.e.* diethyleneglycol), and second, the introduction of the targeted functions through the treatment of the above-mentioned suspension with TEPSA. This previously described procedure[11] allows the introduction of a stable coating layer (formation of a Fe–O–Si covalent bond) with a good control over the layer thickness.

Surface silanisation was characterized by an increase in the hydrodynamic diameter (HD). While native SPIONs show a mean HD (intensity-weighted) of 16.2 nm, coated SPIONs

exhibit a HD of 20.6 nm, (Fig. S1†), a difference of 4.4 nm, which corresponds to an increase in the thickness of 2.2 nm (suggesting thus the formation of a thin shell surrounding the particle cores). The surface modifications were confirmed by the ionisation state of the functionalized ferrofluids according to the pH. If a point of zero charge (PZC) around 7 is typically documented for uncoated SPIONs,[25] a PZC around pH 2 was found for TEPSA-coated SPIONs. Taken together, these observations therefore confirm the efficient silanization of SPIONs (Fig. S2†).

Magnetically functionalized hybrid scaffolds were prepared using different approaches. The two kinds of magnetic nanoparticles (MNPs and nMNPs) were incorporated at different stages during the scaffold preparation: before, during and after biomineralization (Scheme 1). The aim was to optimize homogeneity and efficacy of nanoparticle incorporation, as previously described.

We were able to discard, in the first screening stage, three preparation conditions that did not form homogeneous magnetic hybrid scaffolds. Two of them corresponded to the protocols in which the nanoparticles, both MNPs and nMNPs, were mixed with collagen before biomineralization. The presence of the nanoparticles interfered with the formation of the HA and the final products contained only collagen linked to the magnetic nanoparticles. The third unsuccessful protocol was the one in which the hybrid composite was previously prepared and subsequently soaked in a solution containing the naked nanoparticles (nMNPs). In this case the resulting scaffold was visibly inhomogeneous due to precipitation of nMNPs during drying (Fig. S3†). Therefore, only three different samples were thoroughly characterized: Hy(MNPs)S and Hy(nMNPs)S, magnetically functionalized during biomineralization, and HyS (MNPs), magnetically functionalized after biomineralization.

In the following sections we described the characterization carried out on these materials to explore their suitability as magnetic hybrid scaffolds capable of inducing tissue regeneration and allowing its tracking through imaging techniques (MRI).

3.2. Chemical–physical characterization

Compositional evaluation of the mineral phase of the hybrid scaffolds through ICP analysis revealed a calcium deficiency typical of a low crystalline, ion-substituted apatitic nanophase (Table 1) in all hybrid scaffolds.[26,27] Ca^{2+} ions were partially substituted by Mg^{2+} ions, which were present in the mineralization environment. During biomineralization of all hybrid scaffolds, the same amount of magnesium chloride was present (Mg nominal content). This Mg nominal content was set at a 0.05 Mg/Ca molar ratio, which has been described in the literature as adequate to promote the development of a biomimetic apatitic phase.[28] However, a different amount of Mg was incorporated into the different hybrid scaffolds. Compositional analysis revealed that Hy(MNPs)S and Hy (nMNPs)S have a lower Mg/Ca ratio than HyS and HyS(MNPs). One possible explanation could be that some competitive effect takes place between the iron oxide and magnesium, both present when the magnetic functionalization took place, affecting the final ionic ratio. In contrast, when the magnetic functionalization occurred after the biomineralization, it does not influence the formation of the apatitic phase and the Mg/Ca ratio was found to be the same in HyS(MNPs) and HyS.

The iron content of the scaffolds magnetically functionalized during biomineralization measured by ICP showed that not all the iron added to the solution (3 wt%) was incorporated into the scaffold. It is likely that, as the magnetic functionalization and biomineralization both compete for available COOH groups on the surface of the collagen fibers, not all the magnetic nanoparticles available in the solution interacted and were linked to the hybrid slurry. The incomplete functionalization was evident from visual inspection, as the brown color of the mother liquor after the biomineralization reaction revealed the presence of magnetic nanoparticles in the solution for both MNPs and nMNPs. A higher amount of Fe was detected by ICP in the scaffold containing nMNPs. This small difference could be ascribed to a different interaction between hybrid composites with smaller naked nanoparticles on one side and larger activated ones on the other side. Conversely, in HyS(MNPs), with no competition between processes the entire amount of MNPs was absorbed by the scaffold.

XRD spectra (Fig. 2A) revealed broad reflections ascribable to the low crystal order with nanosize apatitic crystallites according to the Powder Diffraction File (PDF) card #09-0432. The low crystallinity detected is an effect of the low synthesis temperature and of the incorporation of foreign ions such as Mg^{2+} in the apatitic structure provoking structural destabilization.[16] Furthermore, the enhanced 002 reflection was clearly visible highlighting the preferential crystal growth within the collagen fibrils, especially along the *c* axis parallel to the collagen molecule axes, confirming the role of an organic phase that constrains the crystal development in the biomineralization process.[29] These multiple effects (ions and organic matrix) made hybrid scaffolds similar to the natural bone niche and played an important role in the influence of bone

Table 1 Chemical composition of HyS, Hy(nMNPs)S, Hy(MNPs)S, HyS(MNPs) obtained from ICP analysis (mean ± SD)

Samples	Ca/P (mol)	Mg/Ca (mol)	Fe/Ca (mol)	(Ca + Mg + Fe)/P (mol)	Fe_{tot}% (w/w)
HyS	1.53 ± 0.06	0.044 ± 0.001	—	1.60 ± 0.07	—
Hy(nMNPs)S	1.46 ± 0.06	0.018 ± 0.001	0.080 ± 0.004	1.60 ± 0.06	1.82 ± 0.07
Hy(MNPs)S	1.49 ± 0.06	0.018 ± 0.001	0.070 ± 0.003	1.62 ± 0.06	1.62 ± 0.04
HyS(MNPs)	1.58 ± 0.07	0.044 ± 0.001	0.158 ± 0.032	1.89 ± 0.13	2.90 ± 0.08

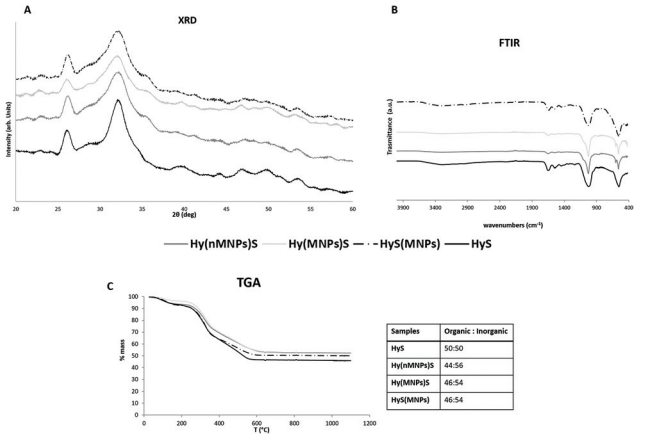

Fig. 2 (A) XRD patterns of the HyS, Hy(nMNPs)S, Hy(MNPs)S, HyS (MNPs). Peaks at 26° and 32° indicates the 002 and 211 reflections; (B) FTIR spectra of the HyS, Hy(nMNPs)S, Hy(MNPs)S, HyS(MNPs); (C) thermal decomposition profile (TG) of the HyS, Hy(nMNPs)S, Hy(MNPs)S, HyS(MNPs): the weight loss in % of mass is used to determine the organic/inorganic ratio of the different samples.

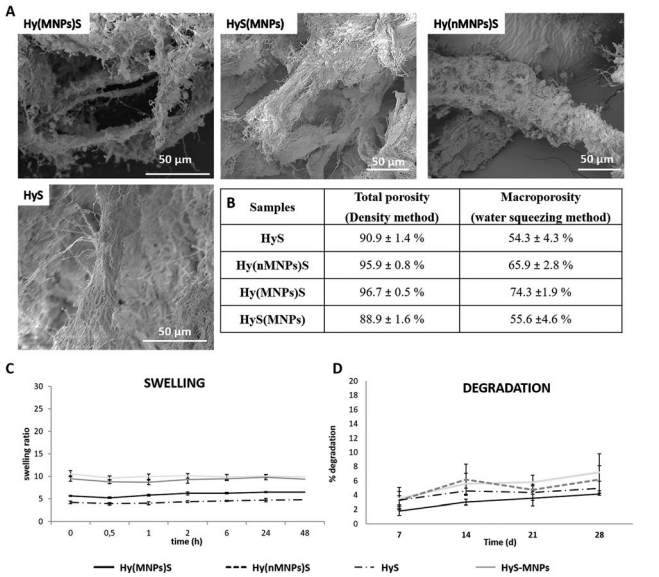

Fig. 3 (A) Scanning electron microscopy images of different composites (HyS, Hy(nMNPs)S, Hy(MNPs)S, HyS(MNPs)); (B) table showing dimensional properties of the composites, total porosity are reported in the middle column and macroporosity in the left column (mean ± SD); (C) time-dependent swelling behavior of hybrid and magnetic composites. *X*-Axis corresponds to time after soaking in PBS, thus the first point is immediately after soaking (mean ± SD); (D) degradation profile of hybrid and magnetic composites after 7, 14, 21, 28 days in PBS buffer (mean ± SD).

metabolism increasing the *in vivo* reactivity and controlling the rate of bone formation and remodeling.[30]

Fourier-Transform Infrared Spectra (FTIR) in Fig. 2B showed the typical pattern of a low crystalline apatite mineralized in the presence of collagen fibers.[16] In detail, the collagen alpha-helical structure was clearly visible in the bands at 1650 cm^{-1}, 1550 cm^{-1} and 1230 cm^{-1} representing the amide I, II, and III. The amide II band is overlapped with the carbonate band of MgHA. Finally, spectra showed the typical absorption bands related to the PO_4 groups at 1032, 565, and 601 cm^{-1}. Generally, band resolution was low for all hybrid composites revealing the typical behavior of non-stoichiometric and low crystalline MgHA, as XRD and ICP had already underlined.

The weight loss detected by thermo-gravimetric analysis (TGA) determined the organic : inorganic ratio (Fig. 2C). Starting from a nominal weight content of 30 : 70 resembling the mineralization extent of natural bone, each hybrid scaffold revealed a lower content close to about 50 : 50. In detail, three different decomposition steps are visible in the graph: from 25 °C to 200 °C one step is associated with water loss and from 200 °C to 600 °C two different steps were detected, associated with the destabilization of collagen chains and fragments and the combustion of organic residues.[9] Different synthetic protocols did not significantly affect the organic : inorganic ratio and the results are compatible with those previously obtained in the ICP analysis, indicating a slightly higher mineral content in Hy(nMNPs)S that revealed a higher amount of iron.

3.3. Structure and morphology of the hybrid scaffolds

Images of the hybrid scaffolds obtained by ESEM microscopy, as shown in Fig. 3A, revealed similar structures in the scaffolds with and without magnetic nanoparticles. All samples showed fibrous micro-architectures with small aggregates of HA closely bound to the collagen fibers, endowing the structures with high micro/macro porosity similar to human trabecular bone.[26] The composite microstructure detected in this study was in compliance with similar mineralized hybrid collagen studied by other authors, showing how, in spite of the functionalization with MNPs/nMNPs, the microstructure was preserved.[26,30]

The table reported in Fig. 3B shows data about total porosity and macroporosity, measured by the density method and the water squeezing method, respectively. Briefly, all samples revealed high total porosity close to 90% and a lower macroporosity close to 60%, since the latter result reveals only the macropore volume percentage instead of overall porosity. However, a slight difference between scaffolds magnetically functionalized during mineralization or afterwards was observed. The latter behaves similar to the non-magnetic scaffold, HyS, indicating that the impregnation with the nanoparticles does not change the porous structure of the previously formed scaffold. On the other hand, the introduction of MNPs/nMNPs during fiber mineralization increased both scaffold porosity and macroporosity. The macroporosity was also sensitive to the type of nanoparticle used. The largest macroporosity was observed in Hy(MNPs)S, where the magnetic nanoparticles covalently attached were previously covered by a TEPSA shell.

The surface carboxylic groups, activated with EDC/NHS chemistry to provide a covalent linkage to the collagen, enlarge

their radius and provide a negative surface charge that could contribute to the expansion of the scaffold pores. Magnetic functionalization with the naked nanoparticles entrapped inside fibers does not have this expanding effect.

Swelling ability is a main parameter to evaluate the capability of the scaffold to absorb PBS and, consequently, cellular medium increasing the permeation of nutrients and their exchange with CO_2 and other metabolites to promote tissue regeneration through cell adhesion and proliferation. All the HyS absorbed immediately a large amount of PBS and the equilibrium saturation was observed after 30 minutes as shown in Fig. 3C. The fast swelling response is a typical feature of highly hydrophilic and porous hybrid scaffolds.[31,32] The introduction of MNPs/nMNPs increased the swelling ratio. Hybrid scaffolds functionalized during mineralization revealed larger swelling ratios, as expected from their higher porosity. Scaffolds functionalized after mineralization showed a swelling ratio similar to HyS, in agreement with the porosity data.

The structural stability of the scaffold is an important parameter to control while developing a scaffold. In order to mimic physiological conditions, the scaffolds were incubated at 37 °C in PBS medium for different time periods (Fig. 3D). The resistance to degradation was evaluated by measuring the weight loss as a function of time. All hybrid composites revealed a good structural stability after 28 days, losing less than 10 wt%. This stability is mainly caused by the presence of a mineral phase that protects collagen from the naturally occurring degradation process that takes place in all hybrid scaffolds.[33] A slight increase in degradation is observed in scaffolds functionalized during mineralization. Their previously described higher porosity facilitates larger water absorption that accelerates degradation. We did not observe any nanoparticle release from the scaffolds even after 28 days, as the PBS solution remained clear. We therefore conclude that the interaction of the nanoparticles, either covalent-bound or mechanically entrapped, remained stable over this period of time.

3.4. Magnetic characterization

The blocking temperature T_B determined as the maximum of the ZFC-FC curves is about 45 K for samples Hy(MNPs)S and HyS(MNPs), which is in agreement with a particle size of ~7 nm (ref. 34) (Fig. S4†). On the other hand, sample Hy (nMNPs)S shows a higher blocking ($T_B \sim 67$ K), which can be related either to larger particles, higher magnetic anisotropy or the presence of dipolar interactions.

The hysteresis loops show a superparamagnetic behavior at room temperature, and at 5 K the systems are blocked. Fig. S5† shows the normalized hysteresis curves at 5 K. It is worth noting two remarkable aspects of these curves: (1) the susceptibility of Hy(nMNPs)S at high field is smaller and (2) the coercive field is higher (see inset Fig. S5†) than the other two. The higher coercive field suggests a higher magnetic anisotropy, which are related to $K_{eff} \sim \mu_0 H_c M_s$, where K_{eff} is the magnetic anisotropy, μ_0 the magnetic permeability of vacuum, H_c the coercive field and M_s the saturation magnetization of the sample. The T_B is related to the magnetic anisotropy K_{eff} and the particle volume V by $T_B \sim K_{eff}V/25k_B$. Therefore, as all the particles have the same size, the higher T_B and H_c for the sample Hy(nMNPs)S suggest that K_{eff} is higher than that for the other samples.

The calculation of the particle size is performed by means of the

Langevin function at low field $\chi_0 = \frac{\mu_0 M_s^2 V}{3k_B T}$, where χ_0 is susceptibility calculated in the linear part of the hysteresis cycle, M_s is the saturation magnetization, V is the particle volume, k_B is the Boltzmann constant and T is the room temperature. As can be seen in Table 2, all the particles have the same size within the experimental error.

As described previously, in Hy(MNPs)S and HyS(MNPs) the nanoparticles are previously modified with TEPSA promoting a covalent bound with mineralized collagen, while in Hy (nMNPs)S naked nanoparticles are introduced in mineralized collagen promoting the physical entrapment of nanoparticles into fibers. Mineralization happens by dropping phosphate acid solution (H_3PO_4) in a calcium basic suspension ($Ca(OH)_2$) through a neutralization process that can induce a reduction at the nanoparticle surface from Fe_2O_3 to Fe_3-xO$_4$-y. Whereas the nanoparticle surface of Hy(MNPs)S is protected by TEPSA and in HyS(MNPs) the neutralization process occurs in the absence of nanoparticles, the naked surface of Hy(nMNPs)S is instantly reduced by calcium hydroxide. This gives place to a kind of core@shell nanoparticle with Fe_2O_3 in the core and reduced Fe_3-xO$_4$-y at the surface. This kind of core@shell structure normally has higher magnetic anisotropy due to the exchange interaction between the core and the shell[35] (Table 2).

3.5 Optimizing the amount of MNPs into the scaffold:Hy (MNPs)S

We prepared some scaffolds with a lower amount of nanoparticles in order to optimize the magnetic signal. Starting from a functionalization of 3 wt% with respect to the hybrid scaffold as previously described, four different samples were studied with 1.5 wt%, 0.75 wt%, 0.37 wt% and 0.075 wt% iron amount and synthesized as previously described reducing only the amount of MNP suspension. From a preliminary observation of reaction products (Fig. 4) the decrease of the amount of MNPs is clearly evident just by looking at the colour of the hybrid slurry and the colour of the mother liquor.

The colour intensity of the hybrid slurries does not vary linearly with the amount of MNPs added during the preparation. Fig. S6A† shows the quantification obtained through ICP. The

Table 2 Particle, particle size, coating or similar, blocking temperature T_B and coercive field H_c (mean ± SD)

Sample	Size (nm)	Coating/or similar	T_B	H_C
Hy(MNPs)S	7.0 ± 0.5 nm	TEPSA	45 K	94 Oe
Hy(nMNPs)S	6.7 ± 0.5 nm	None	67 K	184 Oe
HyS(MNPs)	7.0 ± 0.5 nm	TEPSA	47 K	103 Oe

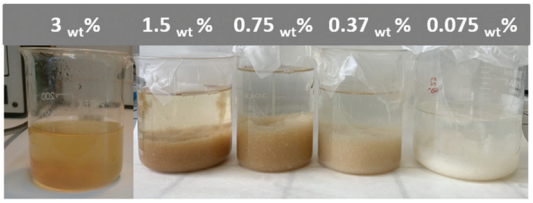

Fig. 4 Picture of the hybrid slurries and mother liquors functionalized with different amounts of MNPs (wt% respect to hybrid collagen).

amount of iron inside the scaffolds decreases non-linearly with the amount of MNPs added during preparation. The functionalization yield, calculated as the ratio between theoretical iron in the hybrid scaffold and effective iron measured by ICP, shows that yields increased with the reduction of MNPs wt% (up to a 96% yield) when only 0.0075 wt% of iron was used to functionalize the scaffold (MNPs_0.0075%). As discussed previously, the functionalization is in competition with biomineralization; thus a low amount of MNPs is easier to link to collagen despite the biomineralization process. Finally, the amount of MNPs did not interfere with the biomineralization process since all scaffolds revealed a similar calcium deficiency, typical of a low crystalline, ion-substituted apatite nano-phase.

TGA analysis shown in Fig. S6B† revealed similar organic : inorganic ratios without any significant differences due to the low amount of MNPs with respect to hybrid scaffolds. Finally, FTIR analysis (Fig. S6C†) in compliance with TGA and ICP highlighted as functionalization with different amounts of MNPs does not interfere with the biomineralization process. The typical pattern of a low crystalline apatite mineralized in the presence of collagen fibers is confirmed for all hybrid scaffolds.

Fig. S7† shows that all scaffolds revealed fibrous microarchitectures with aggregates of small apatitic nanocrystal closely bound to the collagen fibers very similar between them and to human trabecular bone, meaning how in spite of the functionalization with different amounts of MNPs, the microstructure was preserved. Other analyses such as porosity, swelling and degradation show no significant differences from scaffolds previously shown and discussed and therefore they are not presented.

3.6 Magnetic resonance imaging (MRI)

MRI of the different scaffolds has been recorded on a 9.4 T scanner (400 MHz; Fig. 5) using a UTE sequence (TR:5 ms; TE:35 μs). Whatever the labelling method, a strong signal decrease has been observed for all samples when compared to the unlabelled scaffold, confirming thus the efficiency of the labelling processes. However, a strong blooming effect (*i.e.* a signal loss over a larger area) was observed for all magnetically labelled scaffolds, as a consequence of the high local concentration of MNPs within the matrix. This effect was more pronounced when the functionalization was performed after the biomineralization step. It can be assumed that such a labelling

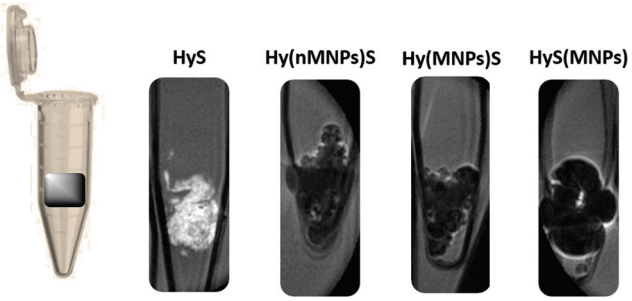

Fig. 5 Comparison of the phantom MR images obtained for the different scaffolds (HyS, Hy(nMNPs)S, Hy(MNPs)S, HyS(MNPs)), using a UTE sequence.

process induces a gradient of MNP' concentration from the edges to the centre of the matrix (*i.e.* a higher MNPs concentration at the edges). Overall, this observation highlights the efficiency of the "one-pot" procedure.[36]

Fig. S8† shows a significant decrease in the signal observed for all samples compared to the unlabelled scaffold, with this decrease appearing linear when the initial iron content increased up to 1.5%. Above this, a saturation of the signal was observed. Interestingly, from a loading of 0.75% MNPs, a real signal enhancement could be observed with a limited blooming effect (Fig. 6).

3.7 Radiolabeling

The uptake of the radiotracer was followed up to 5 h post-incubation, because as it seems from the chromatographic analysis (Fig. 7) provided for the scaffold used as a control (HyS [A]), the hybrid scaffold Hy(MNPs)S with a higher MNP ratio (MNPs_1.5% [B]) and the second magnetic scaffold (MNPs_0.75% [C]), the stability reduces over time with 80–90% of the radiotracer still remaining intact at the longer studied time point. The radiotracer is found at the origin ([^{99m}Tc]Tc-MDP), while any free pertechnetate ([^{99m}Tc]TcO_4^-) moves to the front of the radiochromatograph.

Concerning radiotracer uptake by the scaffolds, it increases in relation to time and there is a trend of higher radiotracer binding affinity towards the scaffold with a higher ratio of loaded MNPs (Fig. 7D).

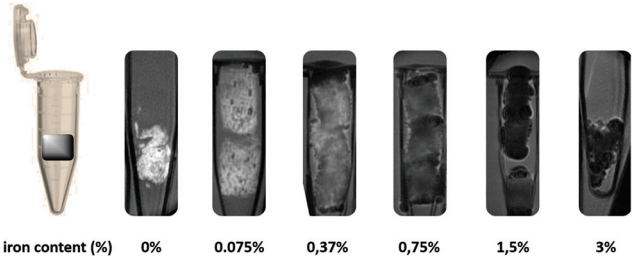

Fig. 6 Phantom MR images illustrating the iron concentration (wt%) dependence on the signal observed for different Hy(MNPs)S scaffolds, using a UTE sequence.

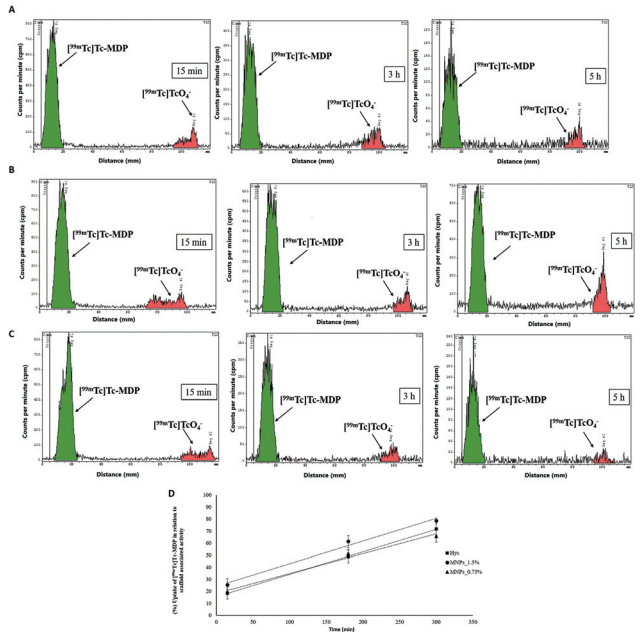

Fig. 7 Radio-TLC of [^{99m}Tc]Tc-MDP tracer, developed on ITLC-SG with methyl-ethyl ketone (MEK) as the mobile phase, following incubation at 37 °C in the presence of scaffolds HyS (A), MNPs_1.5% (B) and MNPs_0.75% (C) at 15 min (left panel), 3 h (middle panel) and 5 h (right panel); (D) binding study of [^{99m}Tc]Tc-MDP after incubation at 37 °C with 3D freeze-dried scaffolds. It represents the percentage of the bound radioactivity in relation to the totally radioactivity associated with the scaffolds. Three different scaffolds were tested HyS as the control; MNPs_1.5% with higher amount of iron; and MNPs_0.75% with lower amount of iron. Results are expressed as the mean of 3 experiments, each performed in duplicate.

[^{99m}Tc]Tc-MDP was found to have high affinity for the inorganic component of the collagen scaffold through the binding of deprotonated oxygen of the phosphonate groups of MDP to the positively charged ions found on it. The higher proportion of tracer uptake by the more magnetically modified scaffold could be attributed to the fact that this type of scaffold had a much more condensed and solid appearance in relation to the other two studied scaffolds. Therefore, this common tracer for bone imaging could be further used for *in vitro* tracking of osteogenic differentiation when these scaffolds are combined with cells before moving to pre-clinical *in vivo* studies. In summary, we showed that we can prepare hybrid scaffolds containing a lower number of nanoparticles. In particular, in this study, we have demonstrated that we can reduce the amount of iron up to 0.75 wt%, thus obtaining a scaffold suitable for bone regeneration labelled with a sufficient amount of MNPs that permit monitoring the progress of bone regeneration *in vivo* through non-invasive imaging techniques, in particular MRI and SPECT/CT.

3.8 Preliminary *in vitro* characterization

The main components of the scaffolds and the synthesized scaffold itself are well known for their lack of cytotoxicity.[30,32,37–39] Nevertheless, we confirmed that the presence of magnetic nanoparticles did not present any unexpected effects on cell viability. To evaluate cytotoxicity, quantitative and qualitative cell viability tests and a cell morphology analysis were performed. The qualitative viability test was performed using the Live/Dead kit, which labels the living cells in green and the necrotic cells in red. The test performed at every time point (1, 3 and 7 days) is reported in Fig. 8A. For all the hybrid composites, the green-marked cells were qualitatively higher in ratio compared to the red-marked cells. The sporadic presence of red-labelled cells is usually observed in a normally growing cell population, suggesting an overall good response of the cells inside the scaffolds containing nanoparticles.

The cell morphology analysis conducted at day 7 *via* labeling the cell cytoskeleton and nuclei with fluorescent probes corroborates the qualitative viability data. The regular shapes of cell nuclei and the stretched cytoskeletons prove the good viability of the seeded cells and absence of any ongoing adverse process (*e.g.* anoikis) (Fig. 8B).

Ultimately, the quantitative evaluation of cell viability was performed by comparing the cells cultured on the scaffolds with nanoparticles with the HyS scaffold, used as the control.

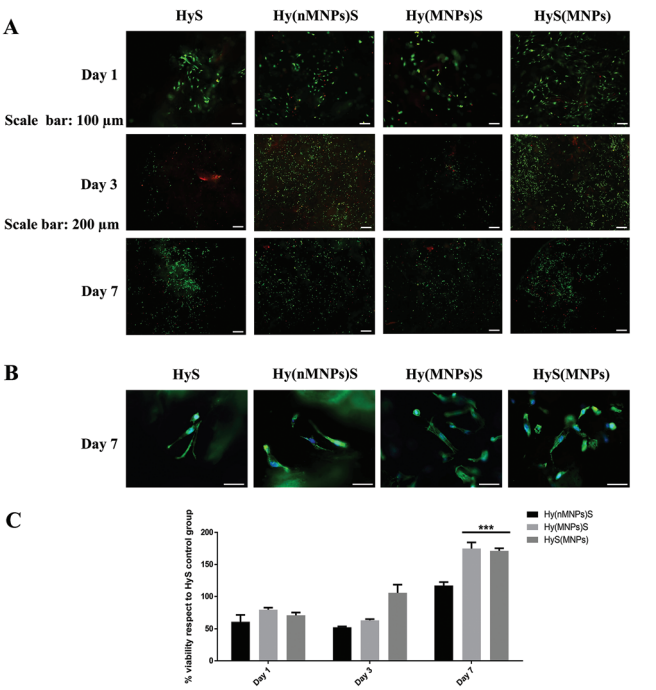

Fig. 8 (A) Qualitative cell viability analysis performed with the Live/Dead kit where Calcein AM labels living cells in green, while Ethidium homodimer-1 labels dead cells in red; (B) cell morphology evaluation test performed at day 7, *via* actin and nuclei staining using phalloidin-FITC and DAPI staining. Overall, the cellular morphologies observed were congruent with the previous experiments, with spread cytoskeletons and round shaped nuclei without irregularities. Scale bar: 200 µm; (C) quantitative viability test performed *via* XTT assay at day 1, 3 and 7 after seeding the cells directly on top of the biomaterials. The graph shows the % of viable cells grown onto the scaffold respect to HyS, used a s a control. At day 7 Hy(MNPs)S and HyS(MNPs) are statistically higher than HyS and Hy(nMNPs)S. ***$P \leq 0.001$; ****$P \leq 0.0001$. Samples $n = 3$; error bars = SEM.

As observed in Fig. 8C, after an initial oscillation of the viability (day 1 and 3), at day 7 both the Hy(MNPs)S and HyS(MNPs) shown a statistically higher viability compared to HyS (****$p \leq 0.0001$). The results indicated that both these scaffolds are statistically different also from Hy(nMNPs)S (***$p \leq 0.001$) suggesting a positive, time-dependent effect induced by the TEPSA-MNPs. No statistical difference has been found between Hy(MNPs)S and HyS(MNPs), meaning that the method of introducing the MNPs (during or after mineralization) did not affect cell viability (Fig. 8C).

The work previously presented allowed us to conclude that the three analyzed magnetic hybrid scaffolds can be considered suitable to provide contrast for performing *in vivo* imaging and boost bone regeneration. However, some differences in the behavior of scaffolds functionalized with MNPs or nMNPs have been noticed. We hypothesize that the surface characteristics of the nanoparticles affect the way they are incorporated into the scaffold. nMNPs have a smaller size but no active surface, while MNPs are larger due to the surrounding activated carboxyl groups needed to promote the covalent linkage with amino or carboxylic groups of the collagen. These surface and size differences can lead to differences in the way they are incorporated: the small size of nMNPs promotes the physical entrapment in larger collagen fibers during fibrils self-assembling whereas the activated shell of MNPs for covalent linkage to the collagen fibers favors their arrangement on their surface, as Scheme S1† shows. This hypothesis is supported by porosity data that show larger pores in Hy(MNPs)S, suggesting the repulsion among the negative surface charges of nanoparticles exposed on the pore surface, thus provoking pore expansion. Conversely, neutral nMNPs could be mainly entrapped inside collagen fibers resulting in a lower porosity. Cytotoxicity assays also support our hypothesis. Cell proliferation in Hy(nMNPs)S is equivalent to that observed in the control scaffolds (HyS), while magnetically functionalized scaffolds with MNPs, introduced during or after biomineralization, show better cell proliferation after 7 days. It has been reported that a magnetic apatitic phase promotes cell proliferation even in the absence of external magnetic fields, but due to a direct contact between cells and magnetic phase.[22,37,40] We can speculate that the reason why a higher cell proliferation was observed only in the functionalization with MNPs is that in this case the magnetic phase is exposed on the collagen fibers and therefore accessible to the cells. Nanoparticles entrapped inside the collagen fibers, Hy(nMNPs)S, are not in contact with cells and therefore cannot stimulate their growth.

Although all magnetic hybrid scaffolds were well-functionalized, we found several reasons to conclude that magnetizing the scaffold during biomineralization is more suitable than magnetizing it at a later stage. Firstly, the soaking procedure creates a less homogeneous magnetization, as we observed a larger deviation in the number of nanoparticles detected by ICP in HyS(MNPs). Furthermore, an additional step is required, which could be a disadvantage to scale-up the production process. In summary, out of the three protocols for preparing magnetic hybrid scaffolds described above, the one that stands out as more convenient is Hy(MNPs)S (functionalization with MNPs during biomineralization process) because it is simple, flexible, therefore more convenient for scaling up the process, and shows the best magnetic and cellular response.

There are, however, other issues that could also be considered when evaluating the magnetized scaffolds. When considering the MRI contrast that the magnetic scaffolds provide, we can also take into account the relation between the amount of iron and the signal intensity. We previously showed that the soaking technique allows higher iron incorporation, 2.9 wt% of iron, as compared to about 1.7 wt% obtained with the simultaneous dropping (Table 1). However, the high amount of iron in HyS(MNPs) saturates the MRI signal, making it not suitable. This result motivated us to explore the possibility of reducing the MNPs content inside the scaffolds to avoid the saturation of the MRI signal and also to minimize, as much as possible, any potential negative effect of the SPIONs. SPIONs are widely used in medicine and biotechnology,[39] but their long-term effect in the human body has lately been under accurate discussion. Although different strategies such as finding new materials endowed with superparamagnetic ability[41] or modifying the surface of these magnetic nanoparticles[42] are being investigated, a conservative approach is to reduce their presence as much as possible. We therefore explored controlling the amount of MNPs on the scaffold and reducing it to the minimum amount needed to provide a reliable detectable MRI imaging signal.

4 Conclusion

A non-cytotoxic and bioresorbable hybrid scaffold composed of hydroxyapatite mineralized on collagen fibers able to induce an osteoinductive signal and boost the regenerative process was successfully functionalized with magnetic nanoparticles (SPIONs). Three different approaches (pre, during and after biomineralization) were explored to achieve the most effective functionalization of the collagen mineralized fibers with naked or modified SPIONs (nMNPs and MNPs). The most interesting results were obtained when the hybrid scaffold (HyS) was functionalized with modified SPIONs simultaneously with the biomineralization procedure (Hy(MNPs)S). The minimum amount of modified SPIONs required to provide a reliable detectable MRI signal, has been optimized thus to minimize any potential negative effect of magnetic nanoparticles. This easy-to-scale procedure results in a MNP-functionalized hybrid composite, which does not show side effects in the cellular response and highlights the required performances for a long time-scale tracking *in vivo*.

Author contributions

Elisabetta Campodoni: conceptualization, performed the experiments, wrote original draft, read and approved the final

manuscript. Marisela Velez: conceptualization, wrote original draft, read and approved the final manuscript. Eirini Fragogeorgi: designed and performed the animal studies, writing, read and approved the final manuscript. Irene Morales: performed the DC magnetic characterization, formal analysis, read and approved the final manuscript. Patricia de la Presa: formal analysis, methodology, data curation, writing, review and editing the manuscript. Dimitri Stanicki: preparation of the nanoparticles, contributed to write the original draft, read and approved the final manuscript. Samuele M. Dozio: conceptualized and performed the biological experiments, wrote original draft, read and approved the final manuscript. Stavros Xanthopoulos: participation in animal studies, validation of radiolabeling and animal experiments. Penelope Bouziotis: validation of radiolabeling experiments, reviewing and editing the final manuscript. Eleftheria Dermisiadou: designated veterinarian in charge of the animals of this study and performed the surgical procedures for the calvarian defect mouse model. Maritina Rouchota: i*n vivo* imaging protocols, SPECT/CT imaging studies, read and approved the final manuscript. George Loudos: supervision of SPECT/CT *in vivo* work and methodologies, read and approved the final manuscript. Pilar Marín: conceptualized the DC magnetic characterization, read and approved the final manuscript. Sophie Laurent: conceptualized the MRI experiments, read and approved the final manuscript. Sébastien Boutry: performed acquisitions of MR images after adequately preparing samples, processed 3D images for displaying comparable views of samples on figures, read and approved the final manuscript. Silvia Panseri: conceptualized the biological experiments, read and approved the final manuscript. Monica Montesi: conceptualized the biological experiments, read and approved the final manuscript. Anna Tampieri: read and approved the final manuscript. Monica Sandri: methodology, conceptualization, read and approved the final manuscript.

Conflicts of interest

The authors declare that there is no conflict to declare.

Acknowledgements

We would like to thank Panopoulos Ioannis, DVM, PhD Director of the Veterinary diagnostic imaging clinic "Alphavet". We would like to acknowledge the Wallon Region (Gadolymph, Prother-Wal and Interreg projects), FNRS and the COST actions and also the Center for Microscopy and Molecular Imaging (CMMI, supported by European Regional Development Found and Wallonia). This project has received funding from the European Union's Horizon 2020 research and innovation program under the Marie Skłodowska-Curie grant agreement no. 645757 and from the Program of Industrial Scholarships of Stavros Niarchos Foundation.

References

1 A. Tampieri, M. Sandri, M. Iafisco, S. Panseri, M. Montesi, A. Adamiano, M. Dapporto, E. Campodoni, S. M. Dozio, L. Degli Esposti and S. Sprio, Nanotechnological Approach and Bio-Inspired Materials to Face Degenerative Diseases in Aging, *Aging Clin. Exp. Res.*, 2021, 805–821, DOI: 10.1007/s40520-019-01365-6.

2 S. Abdulghani and G. R. Mitchell, Biomaterials for In Situ Tissue Regeneration: A Review, *Biomolecules*, 2019, **9**(11), 750, DOI: 10.3390/biom9110750.

3 A. R. Amini, C. T. Laurencin and S. P. Nukavarapu, Bone Tissue Engineering: Recent Advances and Challenges, *Crit. Rev. Biomed. Eng.*, 2012, **40**(5), 363–408, DOI: 10.1615/CritRevBiomedEng.v40.i5.10.

4 E. A. Fragogeorgi, M. Rouchota, M. Georgiou, M. Velez, P. Bouziotis and G. Loudos, In Vivo Imaging Techniques for Bone Tissue Engineering, *J. Tissue Eng.*, 2019, **10**, 2041731419854586, DOI: 10.1177/2041731419854586.

5 S. Sprio, A. Ruffini, F. Valentini, T. D'Alessandro, M. Sandri, S. Panseri and A. Tampieri, Biomimesis and Biomorphic Transformations: New Concepts Applied to Bone Regeneration, *J. Biotechnol.*, 2010, **156**(4), 347–355, DOI: 10.1016/j.jbiotec.2011.07.034.

6 A. Tampieri, S. Sprio, M. Sandri and F. Valentini, Mimicking Natural Bio-Mineralization Processes: A New Tool for Osteochondral Scaffold Development, *Trends Biotechnol.*, 2011, **29**(10), 526–535, DOI: 10.1016/j.tibtech.2011.04.011.

7 L. Preti, B. Lambiase, E. Campodoni, M. Sandri, A. Ruffini, N. Pugno, A. Tampieri and S. Sprio, Nature-Inspired Processes and Structures: New Paradigms to Develop Highly Bioactive Devices for Hard Tissue Regeneration, in *Bio-Inspired Technology*, 2019, DOI: 10.5772/intechopen.82740.

8 S. Sprio, M. Sandri, M. Iafisco, S. Panseri, A. Adamiano, M. Montesi, E. Campodoni and A. Tampieri, Bio-Inspired Assembling/Mineralization Process as a Flexible Approach to Develop New Smart Scaffolds for the Regeneration of Complex Anatomical Regions, *J. Eur. Ceram. Soc.*, 2016, **36**(12), 2857–2867, DOI: 10.1016/j.jeurceramsoc.2016.01.005.

9 A. Tampieri, G. Celotti, E. Landi, M. Sandri, N. Roveri and G. Falini, Biologically Inspired Synthesis of Bone-like Composite: Self-Assembled Collagen Fibers/Hydroxyapatite Nanocrystals, *J. Biomed. Mater. Res., Part A*, 2003, **67**(2), 618–625, DOI: 10.1002/jbm.a.10039.

10 G. B. Ramírez-Rodríguez, J. M. Delgado-López, M. Iafisco, M. Montesi, M. Sandri, S. Sprio and A. Tampieri, Biomimetic Mineralization of Recombinant Collagen Type I Derived Protein to Obtain Hybrid Matrices for Bone Regeneration, *J. Struct. Biol.*, 2016, **196**(2), 138–146, DOI: 10.1016/j.jsb.2016.06.025.

11 J.-L. Bridot, D. Stanicki, S. Laurent, S. Boutry, Y. Gossuin, P. Leclère, R. Lazzaroni, L. Vander Elst and R. N. Muller, New Carboxysilane-Coated Iron Oxide Nanoparticles for Nonspecific Cell Labelling, *Contrast Media Mol. Imaging*, 2013, **8**(6), 466–474, DOI: 10.1002/cmmi.1552.

12 E. Locatelli, L. Gil, L. L. Israel, L. Passoni, M. Naddaka, A. Pucci, T. Reese, V. Gomez-Vallejo, P. Milani, M. Matteoli, J. Llop, J. P. Lellouche and M. Comes Franchini, Biocompatible Nanocomposite for PET/MRI Hybrid Imaging, *Int. J. Nanomedicine*, 2012, **7**, 6021–6033, DOI: 10.2147/IJN.S38107.

13 S. Thomas, Iron Oxide Biomagnetic Nanoparticles (IO-BMNPs); Synthesis, Characterization and Biomedical Applicationâ "A Review, *J. Nanomed. Nanotechnol.*, 2017, 1–9, DOI: 10.4172/2157-7439.1000423.

14 S. Boutry, D. Forge, C. Burtea, I. Mahieu, O. Murariu, S. Laurent, L. Vander Elst and R. N. Muller, How to Quantify Iron in an Aqueous or Biological Matrix: A Technical Note, *Contrast Media Mol. Imaging*, 2009, **4**(6), 299–304, DOI: 10.1002/cmmi.291.

15 B. Kaczmarek, A. Sionkowska, J. Kozlowska and A. M. Osyczka, New Composite Materials Prepared by Calcium Phosphate Precipitation in Chitosan/Collagen/Hyaluronic Acid Sponge Cross-Linked by EDC/NHS, *Int. J. Biol. Macromol.*, 2018, **107**(PartA), 247–253, DOI: 10.1016/j.ijbiomac.2017.08.173.

16 G. S. Krishnakumar, N. Gostynska, M. Dapporto, E. Campodoni, M. Montesi, S. Panseri, A. Tampieri, E. Kon, M. Marcacci, S. Sprio and M. Sandri, Evaluation of Different Crosslinking Agents on Hybrid Biomimetic Collagen-Hydroxyapatite Composites for Regenerative Medicine, *Int. J. Biol. Macromol.*, 2018, **106**, 739–748, DOI: 10.1016/j.ijbiomac.2017.08.076.

17 J. S. Mao, L. G. Zhao, Y. J. Yin and K. De Yao, Structure and Properties of Bilayer Chitosan-Gelatin Scaffolds, *Biomaterials*, 2003, **24**(6), 1067–1074, DOI: 10.1016/S0142-9612(02)00442-8.

18 A. Arora, A. Kothari and D. S. Katti, Pore Orientation Mediated Control of Mechanical Behavior of Scaffolds and Its Application in Cartilage-Mimetic Scaffold Design, *J. Mech. Behav. Biomed. Mater.*, 2015, **51**, 169–183, DOI: 10.1016/j.jmbbm.2015.06.033.

19 M. Ding, K. E. Koroma, J. R. Sorensen, M. Sandri, A. Tampieri, S. M. Jespersen and S. Overgaard, Collagen-Hydroxyapatite Composite Substitute and Bone Marrow Nuclear Cells on Posterolateral Spine Fusion in Sheep, *J. Biomater. Appl.*, 2019, **34**(3), 365–374, DOI: 10.1177/0885328219851315.

20 P. Giorgi, D. Capitani, S. Sprio, M. Sandri, A. Tampieri, V. Canella, A. Nataloni and G. R. Schirò, A New Bioinspired Collagen-Hydroxyapatite Bone Graft Substitute in Adult Scoliosis Surgery: Results at 3-Year Follow-Up, *J. Appl. Biomater. Funct. Mater.*, 2017, **15**(3), e262–e270, DOI: 10.5301/jabfm.5000366.

21 M. E. Mertens, A. Hermann, A. Bühren, L. Olde-Damink, D. Möckel, F. Gremse, J. Ehling, F. Kiessling and T. Lammers, Iron Oxide-Labeled Collagen Scaffolds for Non-Invasive MR Imaging in Tissue Engineering, *Adv. Funct. Mater.*, 2014, **24**(6), 754–762, DOI: 10.1002/adfm.201301275.

22 S. Panseri, C. Cunha, T. D'Alessandro, M. Sandri, G. Giavaresi, M. Marcacci, C. T. Hung and A. Tampieri, Intrinsically Superparamagnetic Fe-Hydroxyapatite Nanoparticles Positively Influence Osteoblast-like Cell Behaviour, *J. Nanobiotechnol.*, 2012, **10**(1), 32, DOI: 10.1186/1477-3155-10-32.

23 A. Tampieri, M. Iafisco, M. Sandri, S. Panseri, C. Cunha, S. Sprio, E. Savini, M. Uhlarz and T. Herrmannsdörfer, Magnetic Bioinspired Hybrid Nanostructured Collagen-Hydroxyapatite Scaffolds Supporting Cell Proliferation and Tuning Regenerative Process, *ACS Appl. Mater. Interfaces*, 2014, **6**(18), 15697–15707, DOI: 10.1021/am5050967.

24 L. Mohammed, D. Ragab and H. Gomaa, Bioactivity of Hybrid Polymeric Magnetic Nanoparticles and Their Applications in Drug Delivery, *Curr. Pharm. Des.*, 2016, 3332–3352, DOI: 10.2174/1381612822666160208143237.

25 D. Forge, S. Laurent, Y. Gossuin, A. Roch, L. Vander Elst and R. N. Muller, An Original Route to Stabilize and Functionalize Magnetite Nanoparticles for Theranosis Applications, *J. Magn. Magn. Mater.*, 2011, **323**(5), 410–415, DOI: 10.1016/j.jmmm.2010.09.031.

26 G. S. Krishnakumar, N. Gostynska, E. Campodoni, M. Dapporto, M. Montesi, S. Panseri, A. Tampieri, E. Kon, M. Marcacci, S. Sprio and M. Sandri, Ribose Mediated Crosslinking of Collagen-Hydroxyapatite Hybrid Scaffolds for Bone Tissue Regeneration Using Biomimetic Strategies, *Mater. Sci. Eng., C*, 2017, **77**, 594–605, DOI: 10.1016/j.msec.2017.03.255.

27 A. Dellaquila, E. Campodoni, A. Tampieri and M. Sandri, Overcoming the Design Challenge in 3D Biomimetic Hybrid Scaffolds for Bone and Osteochondral Regeneration by Factorial Design, *Front. Bioeng. Biotechnol.*, 2020, **8**, 743, DOI: 10.3389/fbioe.2020.00743.

28 A. Tampieri, G. C. Celotti, E. Landi and M. Sandri, Magnesium Doped Hydroxyapatite: Synthesis and Characterization, *Key Eng. Mater.*, 2004, **264–268**, 2051–2054, DOI: 10.4028/www.scientific.net/KEM.264-268.2051.

29 S. R. Stock, The Mineral–Collagen Interface in Bone, *Calcif. Tissue Int.*, 2015, **97**(3), 262–280, DOI: 10.1007/s00223-015-9984-6.

30 A. Tampieri, M. Sandri, E. Landi, D. Pressato, S. Francioli, R. Quarto and I. Martin, Design of Graded Biomimetic Osteochondral Composite Scaffolds, *Biomaterials*, 2008, **29**(26), 3539–3546, DOI: 10.1016/j.biomaterials.2008.05.008.

31 E. Campodoni, E. B. Heggset, A. Rashad, G. B. Ramírez-Rodríguez, K. Mustafa, K. Syverud, A. Tampieri and M. Sandri, Polymeric 3D Scaffolds for Tissue Regeneration: Evaluation of Biopolymer Nanocomposite Reinforced with Cellulose Nanofibrils, *Mater. Sci. Eng., C*, 2019, **94**, 867–878, DOI: 10.1016/j.msec.2018.10.026.

32 C. Menale, E. Campodoni, E. Palagano, S. Mantero, M. Erreni, A. Inforzato, E. Fontana, F. Schena, R. van't Hof, M. Sandri, A. Tampieri, A. Villa and C. Sobacchi, MSC-Seeded Biomimetic Scaffolds as a Factory of Soluble RANKL in Rankl-Deficient Osteopetrosis, *Stem Cells Transl. Med.*, 2018, 1–13, DOI: 10.1002/sctm.18-0085.

33 N. Gostynska, G. Shankar Krishnakumar, E. Campodoni, S. Panseri, M. Montesi, S. Sprio, E. Kon, M. Marcacci, A. Tampieri and M. Sandri, 3D Porous Collagen Scaffolds Reinforced by Glycation with Ribose for Tissue Engineering Application, *Biomed. Mater.*, 2017, **12**(5), DOI: 10.1088/1748-605X/aa7694.

34 P. de la Presa, Y. Luengo, M. Multigner, R. Costo, M. P. Morales, G. Rivero and A. Hernando, Study of Heating Efficiency as a Function of Concentration, Size, and Applied Field in γ-Fe2O3 Nanoparticles, *J. Phys. Chem. C*, 2012, **116**(48), 25602–25610, DOI: 10.1021/jp310771p.

35 P. Crespo, P. de la Presa, P. Marín, M. Multigner, J. María Alonso, G. Rivero, F. Yndurain, J. María González-Calbet and A. Hernando, Magnetism in Nanoparticles: Tuning Properties with Coatings, *J. Phys.: Condens. Matter*, 2013, **25**(48), 484006, DOI: 10.1088/0953-8984/25/48/484006.

36 A. Roch, Y. Gossuin, R. N. Muller and P. Gillis, Superparamagnetic Colloid Suspensions: Water Magnetic Relaxation and Clustering, *J. Magn. Magn. Mater.*, 2005, **293**(1), 532–539, DOI: 10.1016/j.jmmm.2005.01.070.

37 S. Panseri, A. Russo, C. Cunha, A. Bondi, A. Di Martino, S. Patella and E. Kon, Osteochondral Tissue Engineering Approaches for Articular Cartilage and Subchondral Bone Regeneration, *Knee Surg. Sports Traumatol. Arthrosc.*, 2012, **20**(6), 1182–1191, DOI: 10.1007/s00167-011-1655-1.

38 M. Sandri, G. Filardo, E. Kon, S. Panseri, M. Montesi, M. Iafisco, E. Savini, S. Sprio, C. Cunha, G. Giavaresi, F. Veronesi, M. Fini, L. Salvatore, A. Sannino, M. Marcacci and A. Tampieri, Fabrication and Pilot In Vivo Study of a Collagen-BDDGE-Elastin Core-Shell Scaffold for Tendon Regeneration, *Front. Bioeng. Biotechnol.*, 2016, **4**(June), 1–14, DOI: 10.3389/fbioe.2016.00052.

39 L. Mohammed, H. G. Gomaa, D. Ragab and J. Zhu, Magnetic Nanoparticles for Environmental and Biomedical Applications: A Review, in *Particuology*, Elsevier, 2017, pp. 1–14, DOI: 10.1016/j.partic.2016.06.001.

40 S. Panseri, C. Cunha, T. D'Alessandro, M. Sandri, A. Russo, G. Giavaresi, M. Marcacci, C. T. Hung and A. Tampieri, Magnetic Hydroxyapatite Bone Substitutes to Enhance Tissue Regeneration: Evaluation In Vitro Using Osteoblast-Like Cells and In Vivo in a Bone Defect, *PLoS One*, 2012, **7**(6), 1–8, DOI: 10.1371/journal.pone.0038710.

41 A. Tampieri, T. D'Alessandro, M. Sandri, S. Sprio, E. Landi, L. Bertinetti, S. Panseri, G. Pepponi, J. Goettlicher, M. Bañobre-López and J. Rivas, Intrinsic Magnetism and Hyperthermia in Bioactive Fe-Doped Hydroxyapatite, *Acta Biomater.*, 2012, **8**(2), 843–851, DOI: 10.1016/j.actbio.2011.09.032.

42 A. R. Nochehdehi, S. Thomas, M. Sadri, S. S. S. Afghahi and S. M. Mehdi Hadavi, Iron Oxide Biomagnetic Nanoparticles (IO-BMNPs); Synthesis, Characterization and Biomedical Application–A Review, *J. Nanomed. Nanotechnol.*, 2017, **08**(01), 1–9, DOI: 10.4172/2157-7439.1000423.

